Internal report on the channel model from Freeman and Chase.

Loann Terraz[1], **Santiago Eizaguirre**

[1] Light Technology Institute, Karlsruhe Institute of Technology, 76131 Karlsruhe, Germany

Abstract. We report our investigations on the channel model proposed by Freeman and Chase in 1968. We present our way of implementing the model in a MATLAB solver, with the inputs used by the authors as well as more recent ones. We compare the results with numerical simulation and experimental measurements. We include possible uses of the model in the context of atmospheric inductively coupled plasmas.

Contents

1. Introduction

The origin of this study stems from the need of a deeper understanding on how to operate Inductively Coupled Plasma (ICP), and focuses more specifically on optimizing the burner radius for a given set of gas type, coil excitation frequency, coil length and coil distance to the walls. Herein, optimization refers to maximizing the fraction of coil power transmitted to the plasma, while ensuring that the parameters are within operable range and that the plasma would not melt the burner walls. Experiments are one way to gain knowledge in this area, but it is often practically difficult. For instance, studying the influence of the burner radius would require as many experimental setups as variations of said radius. Another more practical way is to use dedicated physics software, like we did with COMSOL Multiphysics® in a companion report. However, numerical calculations suffer from a computational cost increasing with the complexity of the model. Consequently, there is room for a simpler model which would give reliable results when some key parameters are modified, while keeping a low computational cost. Additionally, reducing the number of variables eases the identification of key dependencies, provided that the simpler model was first validated.

In this report we focus on the model derived by Freeman and Chase in 1966, described in [1]. Unlike older but more complete models [2, 3], Freeman *et al.* decided to neglect convected heat and radiation. Considering that, in some cases, radiation heat and convected heat amount for more than 50 % of the total heat (cf. [4] for instance), there is a substantial risk of large errors in this model. It assumes a constant temperature within a cylinder of plasma and is therefore called the "channel model", abbreviated "CM" hereafter. The key equations are described in section 2. The main interest for us is to easily study the influence of the burner radius on the magnetic field strength, the coupled linear power and the plasma radius. Ideally, this would allow us to optimize an ICP setup with different coil lengths, radiuses and operating frequencies.

The work is organized as follows: first, we describe the main equations and how they were implemented on our numerical solver. Then, we discuss the validity of the model, by comparing its results with COMSOL Multiphysics® simulations and actual experiments. Finally, we present some applications and limitations of the channel model.

2. The channel model

Schematically, the plasma torch is modeled as a cylinder of radius R (r-axis), denoted r_0 in figure 1, infinite in the axial direction (z-axis). Inside this burner, the plasma is thought as a finite cylinder of radius r_N ($r_N < R$), denoted r_n in figure 1, and length L, where L is almost equal to the coil length L_{coil} (cf. below). One crude approximation is that the temperature of the plasma, T, is assumed to be constant for any $r <= r_N$. The pressure being fixed to 1 atm in this study, the thermal conductivity k and the electrical conductivity σ only depend on the temperature, hence there are also assumed to be constant in the plasma cylinder.

In terms of heat loss mechanisms only the radial conduction is taken into account. It means that radiation and convection are completely neglected, the latter assumption being probably the largest source of error in the model. The coil losses are also neglected, so that at steady-state the heating from the magnetic field is exactly balanced by the radial conductive losses.

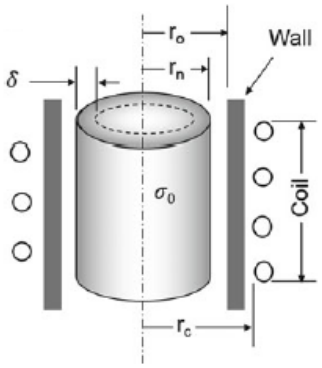

Figure 1. Equivalent channel model representation after the work of [1], reproduced from Boulos *et al* [5].

2.1. Main equations

The model and its equations are extensively detailed in [1]. Here we only report the required inputs, the 3 unknowns to solve and the corresponding 3 independent equations.

2.1.1. Required inputs

- **Geometry:** the burner radius R must be provided. The coil length L_{coil} and distance to the wall are used to estimate the plasma length *via* the "workpiece shortness correction" [6], describing the length for which the magnetic lines are mostly parallel to the axial direction of the burner. We use the Nagaoka factor whose analytical formula in given in [7] to compute the coefficient κ_T such that $L = \kappa_T L_{\text{coil}}$.

- **Gas characteristics:** the thermal conductivity $k(T)$ and the electrical conductivity $\sigma(T)$ must be provided as functions of the gas temperature. These transport properties are widely documented for simple gases like Ar but may prove difficult to find for complex mixtures like Fe-I_2. Note that these two properties are the only quantities having a pressure-dependence in the model.
- **Operation:** the coil excitation frequency ν is required. The plasma/coil power W must be provided. Under the assumptions of the model, $W_{\text{plasma}} = W_{\text{coil}}$.

2.1.2. Variables and main equations

Freeman *et al.* use the heat-flow potential s_0 in their equations rather than the temperature T:

$$s_0(T) = \int_{\tau=0}^{\tau=T} k(\tau) d\tau \tag{1}$$

Because s is a strictly monotonic function of T, solving the model to get s_0 allows, in turn, to obtain the temperature value. The three variables solved are: (i) the heat-flow potential s_0, (ii) the plasma radius r_N, and (iii) the magnetic intensity H_0. Because of the crudeness of the model, Freeman *et al.* claim that only H_0, and possibly r_N, are expected to hold any quantitative interest. The three equations used to solve these variables are numbered respectively (18), (20) and (24) in [1]:

$$\frac{W}{L} = \frac{8\pi H_0^2 \rho F}{\sigma} \tag{2}$$

$$\frac{W}{L} = \frac{-2\pi s_0}{\ln\left(\frac{r_N}{R}\right)} \tag{3}$$

$$\ln\left(\frac{r_N}{R}\right) = -\frac{1}{2} G \frac{\partial \ln \sigma}{\partial \ln s} \tag{4}$$

Here $\frac{W}{L}$ denotes the power per unit of arc length. ρ is the ratio of the plasma radius to the skin depth δ: $\rho = \frac{r_N}{\delta} = r_N\sqrt{\pi\mu\nu\sigma}$, with $\mu = 4\pi \times 10^{-7}\ H.m^{-1}$ the vacuum permeability. F is a function of $(\sqrt{2}\rho)$. With *ber* and *bei* being the real and imaginary parts of the zero-order Bessel function of the first kind with complex argument (also called Kelvin functions), and denoting their derivative with respect to $(\sqrt{2}\rho)$ by a prime, F is written:

$$F(\sqrt{2}\rho) = \sqrt{2}\frac{ber(\sqrt{2}\rho)ber'(\sqrt{2}\rho) + bei(\sqrt{2}\rho)bei'(\sqrt{2}\rho)}{(ber(\sqrt{2}\rho))^2 + (bei(\sqrt{2}\rho))^2} \tag{5}$$

G is derived from F, hence a function of $(\sqrt{2}\rho)$ as well:

$$G = \frac{\frac{\partial \ln F}{\partial \ln \rho} - 1}{\frac{\partial \ln F}{\partial \ln \rho} + 1} \tag{6}$$

2.2. Implementation

The equations are implemented in MATLAB. A large, logarithmically-spaced vector of $\frac{W}{L}$ values is arbitrarily chosen, typically from 10^4 $W.m^{-1}$ to 10^7 $W.m^{-1}$, while all other inputs are set to scalar values. Equations are then solved in a *for-loop* for each value $\left(\frac{W}{L}\right)_i$ of the linear power.

2.2.1. The electrical conductivity and its log-derivative

Numerically, the most sensitive quantity in the equations is the term $\frac{\partial \ln \sigma}{\partial \ln s}$, appearing in eq. 4. Whether it comes from a graphic fit or tabulated data, any small oscillation of $\sigma(T)$ results in drastic variations of $\frac{\partial \ln \sigma}{\partial \ln s}(s_0)$. This term can take non-consistent values, particularly at low s_0, but it is usually out of the range of interest because the corresponding temperature is too low for a steady-state plasma. Consequently, we introduced a minimum value $s_0^{\min}$ to avoid numerical issues, although by definition the minimum should be 0 $W.m^{-1}$. Similarly, we introduced a maximum value $s_0^{\max}$ corresponding to the maximum temperature given in our data tables. While using the data extracted from [1] for N_2 we found out the need to artificially set $\frac{\partial \ln \sigma}{\partial \ln s}$ to 0 at $s_0^{\max}$, or else no solution was found at the highest linear power values. More detail about the influence of $\frac{\partial \ln \sigma}{\partial \ln s}$ is given in section 3 and section 4.

2.2.2. Spacing the variable r_N

We define the reduced plasma radius $u = \frac{r_N}{R}$ and space it over a thousand points. Rather than spacing it over the range $[0; 1]$, we define the boundaries $u_i^{\min}$ and $u_i^{\max}$, defined for each $\left(\frac{W}{L}\right)_i$ value thanks to equation 3:

$$u_i^{\min} = \exp\left(\frac{-2\pi s_0^{\max}}{\left(\frac{W}{L}\right)_i}\right) \tag{7}$$

$$u_i^{\max} = \exp\left(\frac{-2\pi s_0^{\min}}{\left(\frac{W}{L}\right)_i}\right) \tag{8}$$

2.2.3. Solving the equations

From the 1×1000 vector of "guess" values for r_N and eq. 3, we derive a 1×1000 vector of "guess" values for s_0. The variables ρ, $F(\sqrt{2}\rho)$ and $G(\sqrt{2}\rho)$ are then evaluated for the 1000 points. The corresponding eq. 4 is evaluated and the best couple $\{r_N; s_0\}$ is selected. Finally, the calculated values are used in eq. 2 to obtain H_0. This process is repeated for each value of the vector $\frac{W}{L}$. Assuming a resolution of 1000 points for $\frac{W}{L}$, it takes ≤ 5 s to compute results for one set of frequency ν, burner radius R and gas type. This has to be compared with COMSOL simulations' computational time, which ranges from a few minutes to several days.

2.3. Discussion

2.3.1. Numerical factors

While implementing the code to solve equations 2, 3 and 4, it appeared that the results shown in [1] are well reproduced if and only if the right terms of equation 2 are multiplied by a factor of 2. Consequently, it was implemented as:

$$\frac{W}{L} = \frac{16\pi H_0^2 \rho F}{\sigma} \tag{9}$$

Similarly, we found that equation (23) in [1] has a mistake, but the derived equation (25) is correct, so it does not change the final results.

Another question arises when checking the numerical factors in the 3 papers ([1, 2, 3]) using eq. 2. The use of CGS units in [2] makes direct comparison troublesome, so we focus on the equation numbered (12) in [3] instead. After changing the variable names and checking the definition of function $Q(\kappa)$ in [2], it seems that the factor 8 in eq. 2 is missing in [3].

2.3.2. Domain of validity of ρ

Freeman *et al.* discussed the possible numerical values of the reduced parameter ρ:

> "An interesting constraint arises from (~~14~~ 24) and (~~15~~ 25). That is, the derivative in (~~14~~ 24) is necessarily positive while the logarithmic term is necessarily negative. Therefore, no solutions are possible with negative values of G. As this crossover occurs at about $\rho = 1.75$, [...]"

In our code, $G(\sqrt{2}\rho)$ is indeed becoming negative after the threshold $\rho \simeq 1.78$, but the term $\frac{\partial \ln \sigma}{\partial \ln s}$ in eq. 4 is always positive only when $\sigma(T)$ is an increasing function vs T. It is the case for argon and nitrogen within our range of temperature, but becomes false for $T \geq 20000\ K$ for example. There may be other gases for which the electrical conductivity is not monotonic below $T < 15000\ K$.

2.3.3. Multiple solutions

[Corresponding report: 11^{th} of September 2024.]

For some values of linear power $\frac{W}{L}$, up to 3 couples $\{r_N; s_0\}$ can satisfy eq. 2 3 and 4, when the gas is N_2. Freeman *et al.* also mention this in their publication, but do not make assumptions regarding the physical viability of these solutions. This is due to the non-monotonic shape of $k(T)$ for N_2, as it splits into N atoms for $T \geq 5000\ K$. Consequently, $\sigma(s_0)$ shows a maximum slope around $s_0 \simeq 22000\ W.m^{-1}$ and $\frac{\partial \ln \sigma}{\partial \ln s}$ has a peak around this value. This non-linear effect allows for more than one solution when solving the equations.

For the sake of simplicity, we decided to keep only one solution. The criteria was set to be the continuity of the parameter ρ, because it depends on both r_N and s_0. Nonetheless, the transition between a linear power region where there is only one solution and one where more than one solution exists leads to discontinuities.

2.3.4. Asymptotic behavior

[Corresponding report: 25th of July 2024.]

From eq. 3, we see that a high linear power corresponds to plasma radius close to the burner radius, which is quite intuitive. Consequently, the left hand-side term in eq.4 tends to 0. Although we artificially created a value $s_0^{\max}$ such that $\frac{\partial \ln \sigma}{\partial \ln s}(s_0^{\max}) = 0\ S.W^{-1}$, physically there is no reason for this term to do so. Consequently, while considering eq. 4, the term on the right-hand side is null if and only if $G(\sqrt{2}\rho) = 0$, which occurs at $\rho = \rho_{\lim} \simeq 1.78$. This defines an asymptotic behavior for curves at high linear powers, where $r_N \to R$ and $\rho \to \rho_{\lim}$. It can also be used to define $H_0^{\lim}(W/L)$ and an electrical conductivity limit:

$$\sigma_{\lim} = \left(\frac{\rho_{\lim}}{R}\right)^2 \frac{1}{\pi\mu\nu} \tag{10}$$

Interestingly, this limit does not depend on the gas type, so that argon, nitrogen or oxygen will exhibit the same H_0 values at high linear powers for a given burner radius and frequency. However, the corresponding temperature is gas-dependent. Within the range of parameters we use in this report $\sigma_{\lim}$ has very low values, which are usually not consistent with COMSOL simulations.

3. Validation

3.1. Reproducing the previous results

Figure 2 shows a comparison between the results obtained with our code and the extracted data from figure 5 in [1]. The transport properties of argon and nitrogen were directly extracted and interpolated from the figures given in [1]. The burner radius is fixed at $R = 1.27 \times 10^{-2}\ m$ (1 *inch* diameter). The overall agreement is good, especially for argon. A few points stand out because of the multiple solutions issue mentioned in the previous section. It also explains why the curve trends deviate from the extracted data, as the solution we selected is different from the one plotted by Freeman and Chase.

One can multiply the abscissa of the minimum of each curve by the plasma length L to obtain the minimum sustaining power (MSP), as described in [8]. By using electronic considerations, the authors argue that the left hand side of the minimum does not correspond to an operable plasma in practice. Comparisons with experiments in the early '70s led to the conclusion that the MSP prediction is satisfactory while the corresponding minimum magnetic intensity can be underestimated by one order of magnitude.

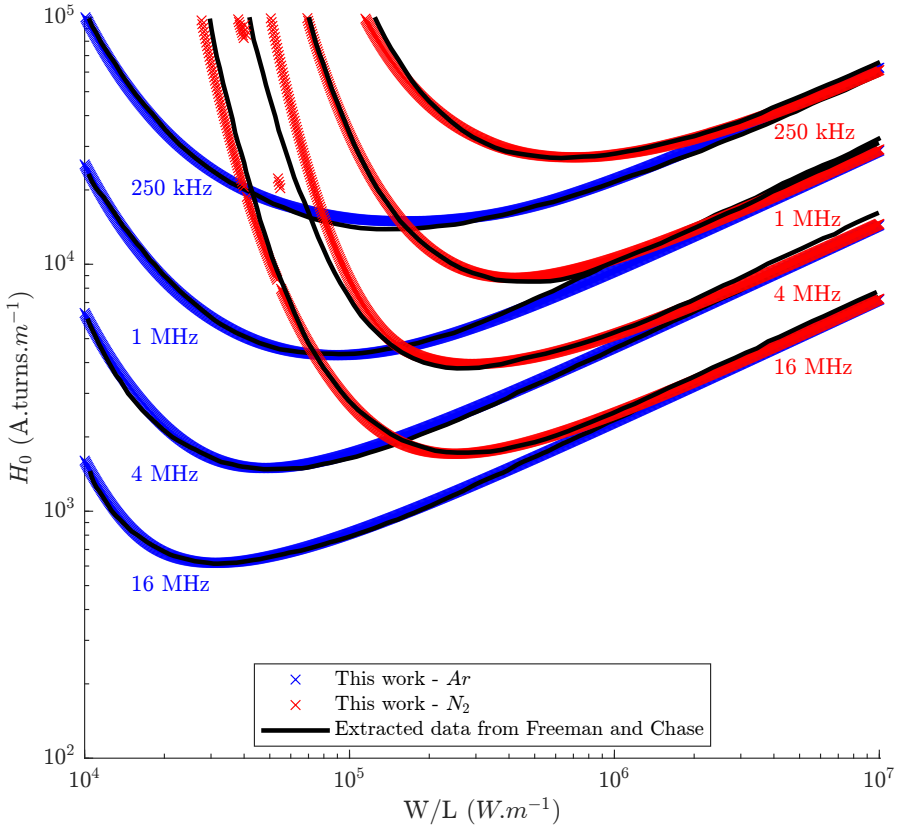

Figure 2. Comparison between this work and the results presented in [1].

3.2. Comparisons with recent experimental results

3.2.1. Argon ICP at 13.56 MHz

[Corresponding report: 06th of June 2024.]

An atmospheric ICP argon plasma was run at different excitation currents in the laboratory. Only the sheath inlet was used to inject the gas. The fixed parameters are shown in table 1, while the current I_{RMS}, voltage V_{RMS} and plasma input power P_{in} (generator input power minus coil losses) are shown in table 2. Voltage and current are given as root mean square (RMS) values, while the equations use peak values, with the simple relation: $X_{peak} = \sqrt{2}X_{\mathrm{RMS}}$. Quantities without subscript correspond to peak values in this report.

Table 1. Constants for the experiments

Gas	ν (MHz)	L_c (mm)	R_c (mm)	N	R (mm)	Q_{sheath} $(L.min^{-}1)$	Q_{center} $(L.min^{-}1)$
Ar	13.56	75	39.5	3	30	30	0

Table 2. Variables for the experiments

I_{RMS} (A)	V_{RMS} (V)	P_{in} (W)
20.70	1218	939
21.93	1267	1129
24.01	1365	1390
25.95	1456	1591
27.89	1547	1803
29.67	1630	1981
31.38	1708	2183
32.95	1780	2338
34.33	1843	2456

Figure 3 shows the results of the experiments compared with the results of the channel model. Two data sets are used: one with the thermal conductivity k and electrical conductivity σ used by Freeman *et al.*, and one using the data available in COMSOL (which refers to Boulos *et al.* [5]). The magnetic intensity H is estimated by two different ways: the peak current multiplied by the coil turn density (similar to [1]), or through simple COMSOL simulations where only the relevant geometry and the magnetic field are modeled to get a field $B(I_{peak})$, averaged over the "plasma volume" $V = \pi R^2_{\mathrm{burner}} \kappa_T L_{\mathrm{coil}}$. The power measurements P_{in} are used to compute the linear power (*i.e.* the abscissa on figure 3) such that $W/L = P_{in}/(\kappa_T L_{\mathrm{coil}})$.

The CM results with COMSOL inputs are different by a factor 4 to 5 from the experimental H_0 estimated *via* B. Both curves are increasing, but the slope of the measurements is greater than the theoretical one. CM results from Freeman inputs seem off as the experimental points cross the theoretical MSP.

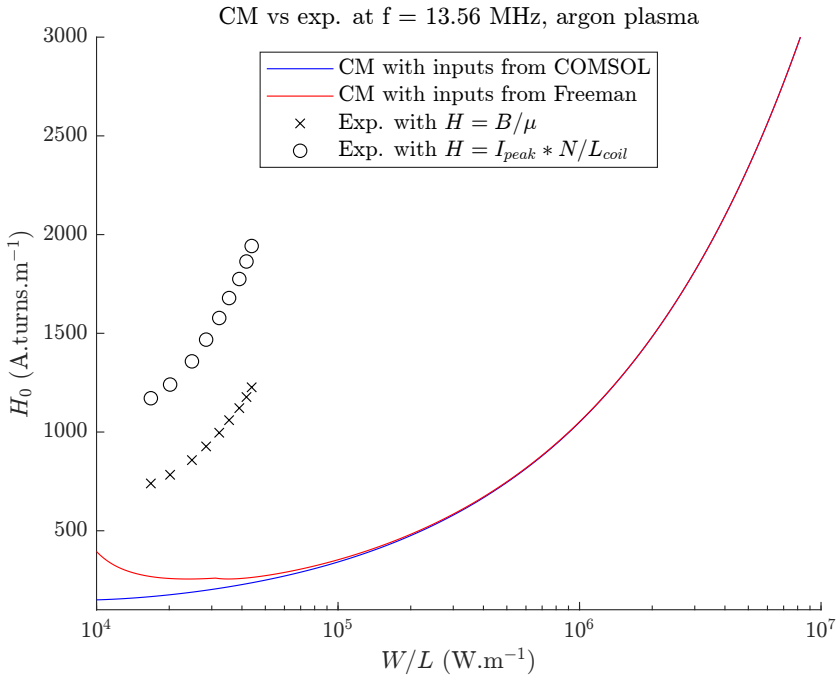

Figure 3. Comparison between channel model and experiments for a 13.56 MHz atmospheric ICP argon plasma.

The MSP for different gas flow rates were measured experimentally, cf. table 3. Because the CM does not include gas flow rates in the equations, only one corresponding MSP is derived from the model: $P_{CM} = 472\,W$. This value is about twice lower than the MSP for $Q \in [20; 50]\ L/min$, so the agreement is rather poor. However, the uncertainty of the measurements is also large and should not be trusted too much in this specific case. A simple COMSOL simulation with only a center inlet was run to add data to the comparison. While the dependency on the flow exists, its influence seems lower than the experimental results and the trend is the opposite. However, the discrepancy with the CM results is greater than a factor 5, so the agreement is not good.

Table 3. Experimental and numerical MSP for argon at 13.56 MHz.

Q $(L.min^{-}1)$	15	20	25	30	35	40	45	50
P_{exp} (W)	1550	903	886	866	800	826	785	736
P_{COMSOL} (W)	2300	2400	2400	2500	2500	2600	2600	2700

3.2.2. Argon ICP at 165.1 kHz

[Corresponding reports: 20th of June and 18th of July 2024.]

Similarly to the previous case, we report the constants used during the experiment and their corresponding simulations in table 4. In this case we have only one measurement, represented by the black cross in figure 4. In contrast to the previous example, the COMSOL simulations used to get $B = \mu H_0$ are much more detailed,

taking into account gas flow, wall thickness, coupling with heat and laminar flow, etc. The experimental point differs by almost a factor 10 from the CM predictions. The magnetic intensities from COMSOL simulations are about 4 times greater than CM predictions. Note that the slope is well reproduced this time, contrary to the 13.56 MHz case.

Table 4. Constants for the experiment and corresponding simulations

Gas	ν (kHz)	L_c (mm)	R_c (mm)	N	R (mm)	Q $(L.min^{-1})$
Ar	165.1	101	57.5	4	47.5	100

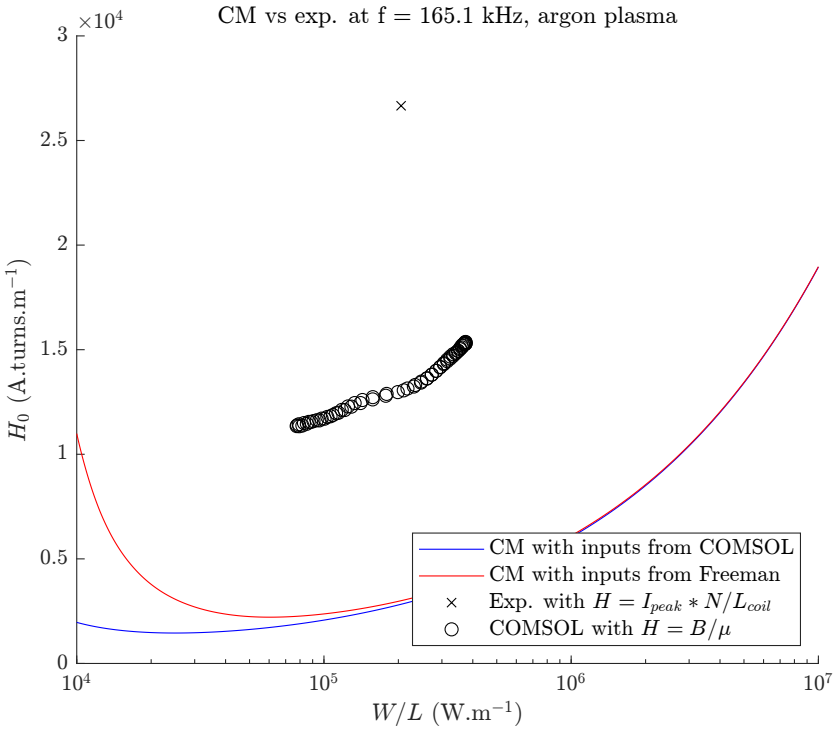

Figure 4. Comparison between channel model, COMSOL and one experiment for a 165.1 kHz atmospheric ICP argon plasma.

3.3. Comparisons with COMSOL simulations for the MSP

3.3.1. MSP of nitrogen ICP for varying burner radiuses at 2.1 MHz and 6 MHz

Here we present a comparison between COMSOL simulations and CM predictions. We focus on the MSP, but we also report the maximal temperature along the axis of symmetry, labeled "core temperature" hereafter, that is $T_{max} = \max(T(z, r = 0))$, where z is the coordinate in the axial direction. The numerical model does not include radiation. The MSP was estimated by ramping down the coil power excitation, including plateaus at each step, to ensure that steady-state is reached. The power step is equal to 500 W for the 2.1 MHz case and 357 W for the 6 MHz case. Table 5 shows

the geometrical and flow parameters used in COMSOL. The burner radius varies from 50 mm to 120 mm by increments of 10 mm. The gap between the burner radius and the coil is kept at the constant value of 7 mm.

Table 5. Parameters for the simulations, $\nu = \{2.1\ MHz\ ;\ 6\ MHz\}$

Gas	$L_c\ (mm)$	N	$R_c\ (mm)$	$R\ (mm)$	$Q\ (L.min^{-}1)$
N_2	100	5	$R+7$	varying	100

Figure 5 shows the evolution of MSP predictions vs burner radius. Error bars appearing in COMSOL data correspond to the step size between 2 power plateaus ; no other uncertainties were considered. The MSP decreases with the burner radius, at constant coil gap, and with the frequency, which is expected. The curve trend is well reproduced by the channel model, and the relative difference is below 8% for the 2.1 MHz case, while it is about 20% for the 6 MHz case. Within the conditions of this study, the CM could be used as a rough estimation of the MSP.

Figure 6 was plotted with the same conditions but displays the constant temperature from the CM, compared with the temperature at the center of the coil and $r = 0$. The results from COMSOL are time-dependent, so we choose to display the core temperature at steady-state when $P_{\text{coil}} = MSP$. The agreement for the 2.1 MHz case is surprisingly good, which also means that the CM overestimates the average temperature along the radial axis, as T typically goes down to reach room temperature at $r = R$. However, the channel model can then be used as a predictive tool to estimate the core plasma temperature, which can prove useful. At 6 MHz, the trend differs between the two models, but the absolute values are relatively close.

3.3.2. MSP of argon ICP for varying burner radiuses at 2.1 MHz

The results presented here are obtained with the same conditions as the previous section (cf. table 6), except that it is for argon and there is only one frequency: $\nu = 2.1\ MHz$.

Figure 7 shows MSP comparisons between COMSOL and CM. Contrary to the N_2 case, the agreement is not good and the trend is not respected. Surprisingly, the required power to sustain plasma discharge is increasing vs burner radius in COMSOL simulations. The agreement is better for the temperature comparison, shown in figure 8. The discrepancy is constant and about 2300 K. The fact that the core temperature in COMSOL is higher than CM prediction is also expected.

Table 6. Parameters for the simulations, $\nu = 2.1\ MHz$

Gas	$L_c\ (mm)$	N	$R_c\ (mm)$	$R\ (mm)$	$Q\ (L.min^{-}1)$
Ar	100	5	$R+7$	varying	100

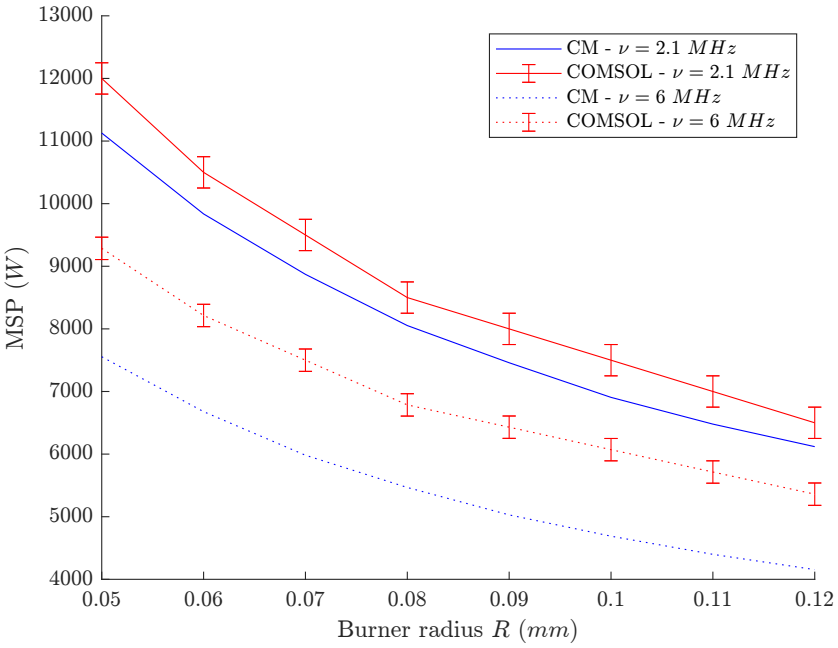

Figure 5. MSP predictions with CM and COMSOL for an atmospheric nitrogen ICP with burner radius variations. Full lines correspond to 2.1 MHz and dots to 6 MHz.

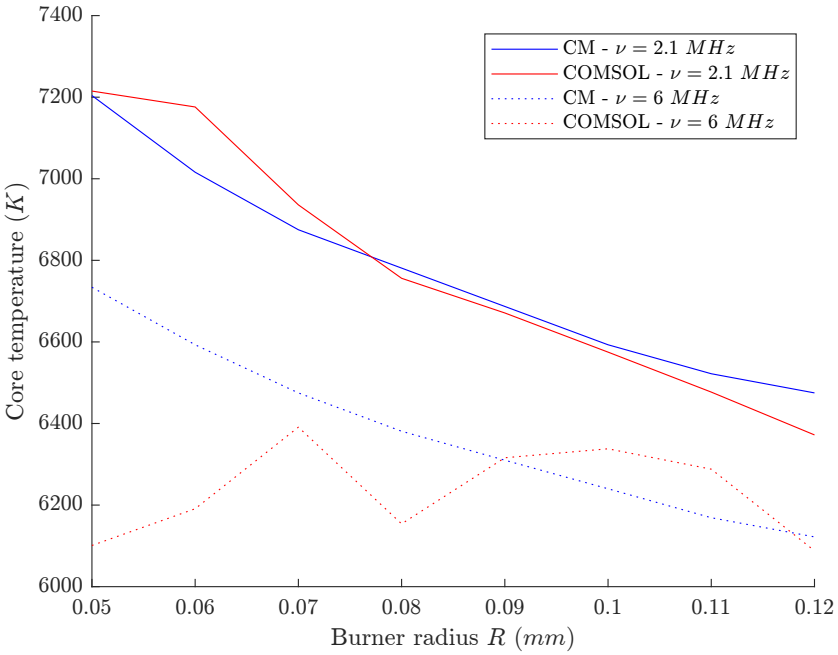

Figure 6. Core temperature predictions with CM and COMSOL for an atmospheric nitrogen ICP with burner radius variations. Full lines correspond to 2.1 MHz and dots to 6 MHz. Temperatures from COMSOL correspond to a steady-state at $P_{\text{coil}} = MSP$.

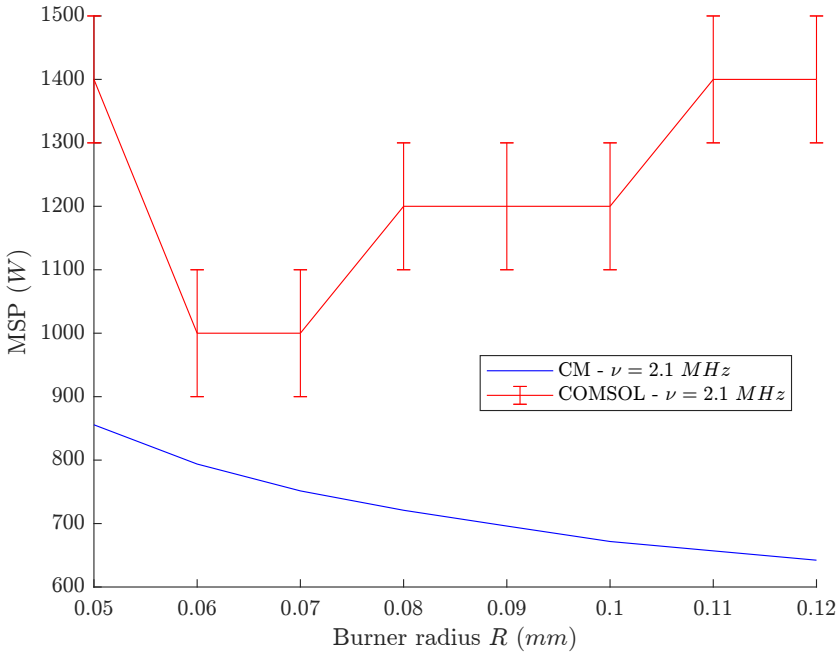

Figure 7. MSP predictions with CM and COMSOL for an atmospheric argon ICP with burner radius variations, at $\nu = 2.1\ MHz$.

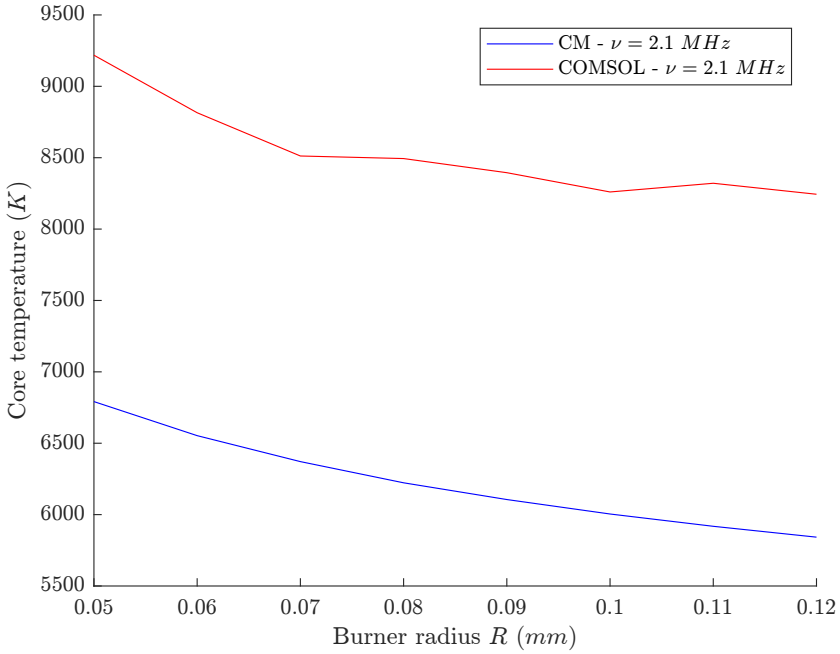

Figure 8. Core temperature predictions with CM and COMSOL for an atmospheric argon ICP with burner radius variations, at $\nu = 2.1\ MHz$. Temperatures from COMSOL correspond to a steady-state at $P_{\text{coil}} = MSP$.

4. Applications: plasma radius and coupling coefficient

4.1. Definitions

Hereafter we discuss the plasma radius r_N, the electrical conductivity σ and the temperature T. The plasma radius definition from the CM is clear: it is the limit of the homogeneous plasma cylinder. However, the definition of a plasma radius in actual experiments or in numerical simulations is rather subjective. When the gas is emitting visible light, the radius can be optically estimated as the limit between the transparent and the colored regions. From numerical studies, it can be defined either with a temperature threshold, or the position ($\pm\delta/2$) where the maximum power from the magnetic field is deposited. In the following parts of this report, plasma radius definition will always be explicitly detailed. Knowing the plasma radius is of interest to estimate how close the plasma is to the burner walls (with the risk of damaging them), but also to estimate the coupling coefficient ξ. Following the definition given in [3], this coefficient characterizes the transfer of power from the coil to the discharge:

$$\xi = \frac{\overline{W_D}}{\overline{W_R}} = \frac{\left(\frac{r_N}{R_c}\right)^2 Q}{1 - \left(\frac{r_N}{R_c}\right)^2 (1 - P)} \tag{11}$$

where $\overline{W_D}$ is the discharge power, $\overline{W_R}$ is the reactive power, Q and P are the dimensionless real and imaginary parts, respectively, of the complex flux integral over the discharge area (cf. [2]). Q and P are functions depending on a parameter $\kappa = \sqrt{2} r_N/\delta = \sqrt{2}\rho$. At low r_N/R_c values, the coupling coefficient ξ peaks at $\kappa = 2.5$, while at higher values the maximum is shifting to the right. It means that optimum coupling is reached when $r_N \gtrsim 1.77 * \delta$. Following the same example as the one p. 856 in [5], for a 1 MHz argon plasma operating at the average temperature of 8000 K, the skin depth is equal to $\delta = 16$ mm. Consequently, the plasma radius for optimum coupling is about 28.3 mm, setting a minimum value for the burner radius. In comparison, a nitrogen plasma at the same temperature and frequency would have an optimum radius of 33.9 mm. Figure 9, extracted from [3], shows the evolution of ξ vs κ at different r_N/R_c ratios.

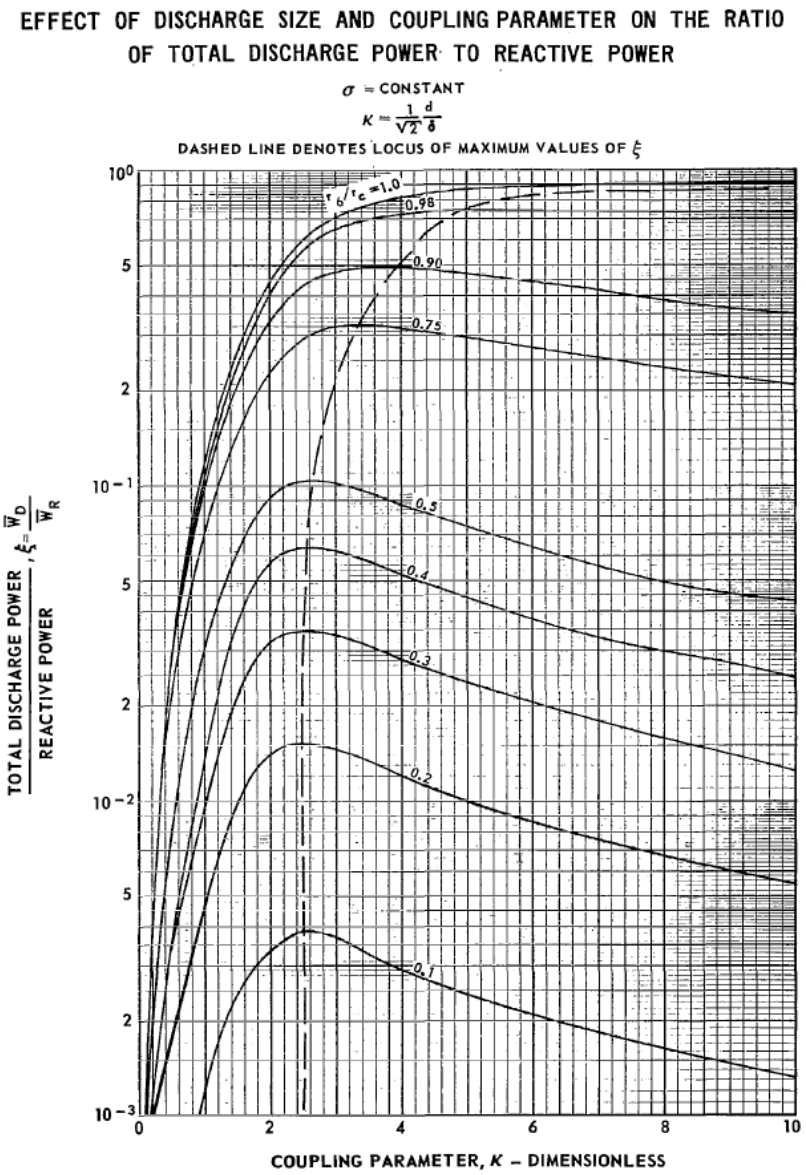

Figure 9. Extracted figure from [3].

4.2. Comparison between COMSOL results and CM: 175 kHz *argon case*

[Corresponding report: 18th of July 2024.]

In this section we want to compare the plasma radius r_N, the electrical conductivity σ, and their derived quantities (skin depth δ and T). The context of the study is the same as the one presented in 3.2.2. The corresponding COMSOL simulation, performed by S. Eizaguirre, have a constant inlet volume flow rate of 100 $L.min^{-1}$. The above-mentioned quantities are calculated at 10 different cutlines, numbered 1 for the closest to the inlet and 10 for the furthest (cf. figure 10).

The COMSOL study is a transient one with varying excitation current vs time. Figure 11 shows the power coupled into the plasma for the different current values. A typical hysteresis appears: the curve obtained when the current is ramped up does not

Figure 10. Cutlines at which the plasma parameters are calculated. The lowest is numbered 1, while the highest is numbered 10.

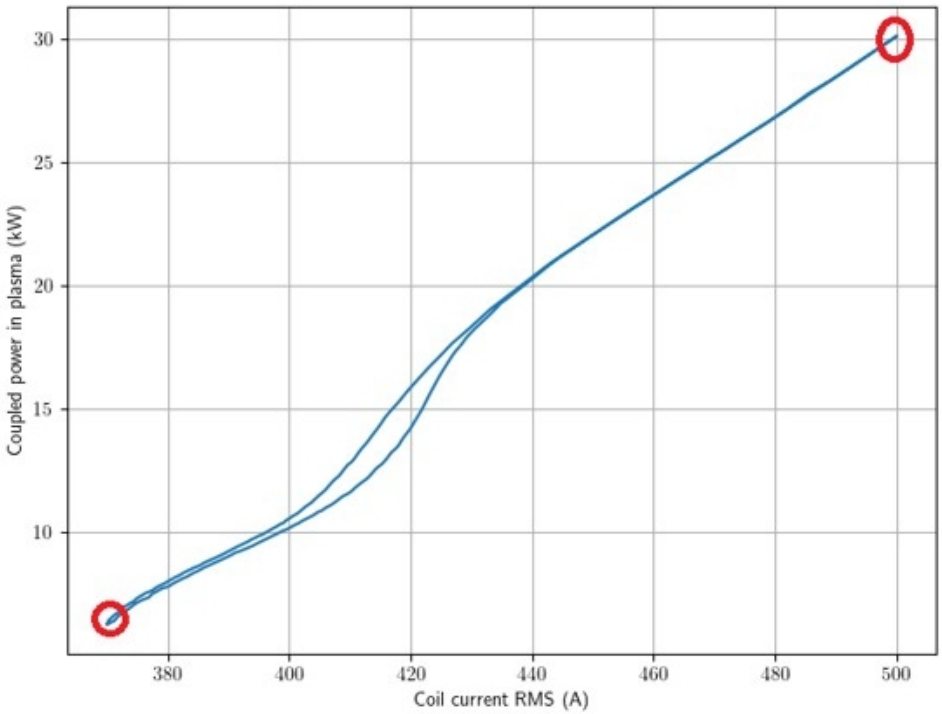

Figure 11. Coupled power vs excitation current (RMS). The current is first ramped up, then ramped down. The red circles show at what current value the plasma parameters are calculated for the 10 cutlines.

exactly overlap the curve obtained when the current is ramped down. In this study, we are interested in the two extreme points of the curve: the minimum value and the maximum value, at 370 A and 500 A respectively. From the channel model point of view, the cutline position does not matter. However, the linear power (*i.e.* the abscissa in typical figures like 2, 3 and 4) is changing because the coupled power is not the same. This is illustrated in figure 12.

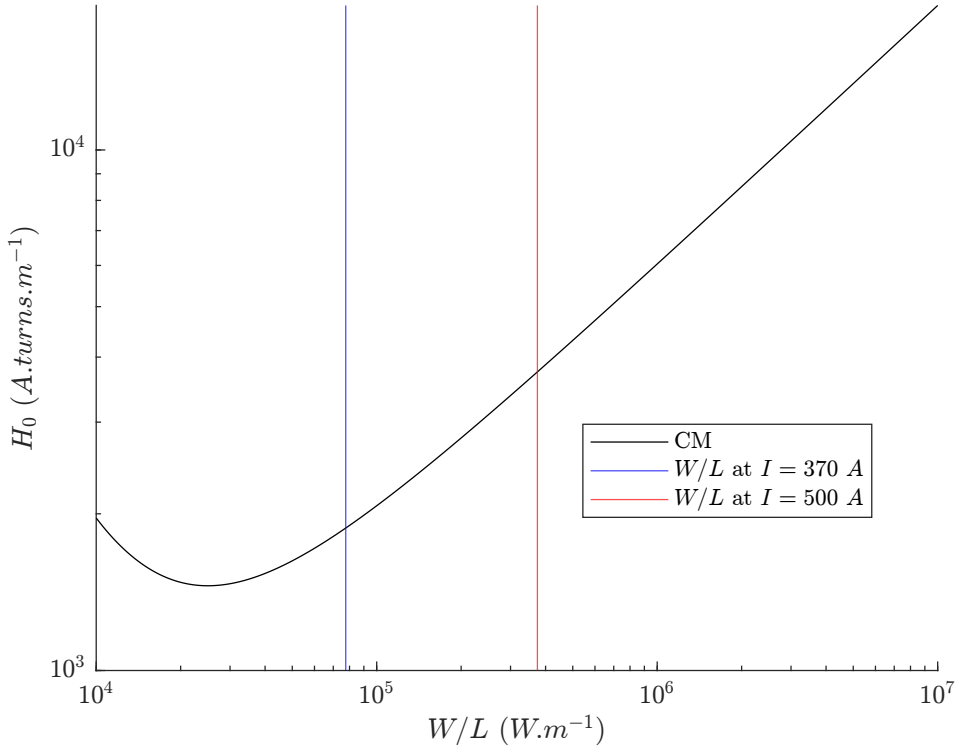

Figure 12. H_0 (black) with the linear powers at 370 A (blue) and at 500 A (red) represented.

Here, we choose to define the plasma radius from COMSOL as the radial position where the maximum power is deposited from the magnetic field. The skin depth is defined as the length required to reduce the maximum by $\exp(-1)$ (relatively). The temperatures and the electrical conductivities along the cutlines are averaged from $r = 0$ mm to $r = r_N$. Results are presented in figure 13. Apart from the plasma radius, the quantities derived from the channel model are almost the same for the two linear powers, which is definitely a drawback of the model. The absolute agreement with COMSOL values is also poor, preventing the use of this simplified theory from prediction purposes in this context.

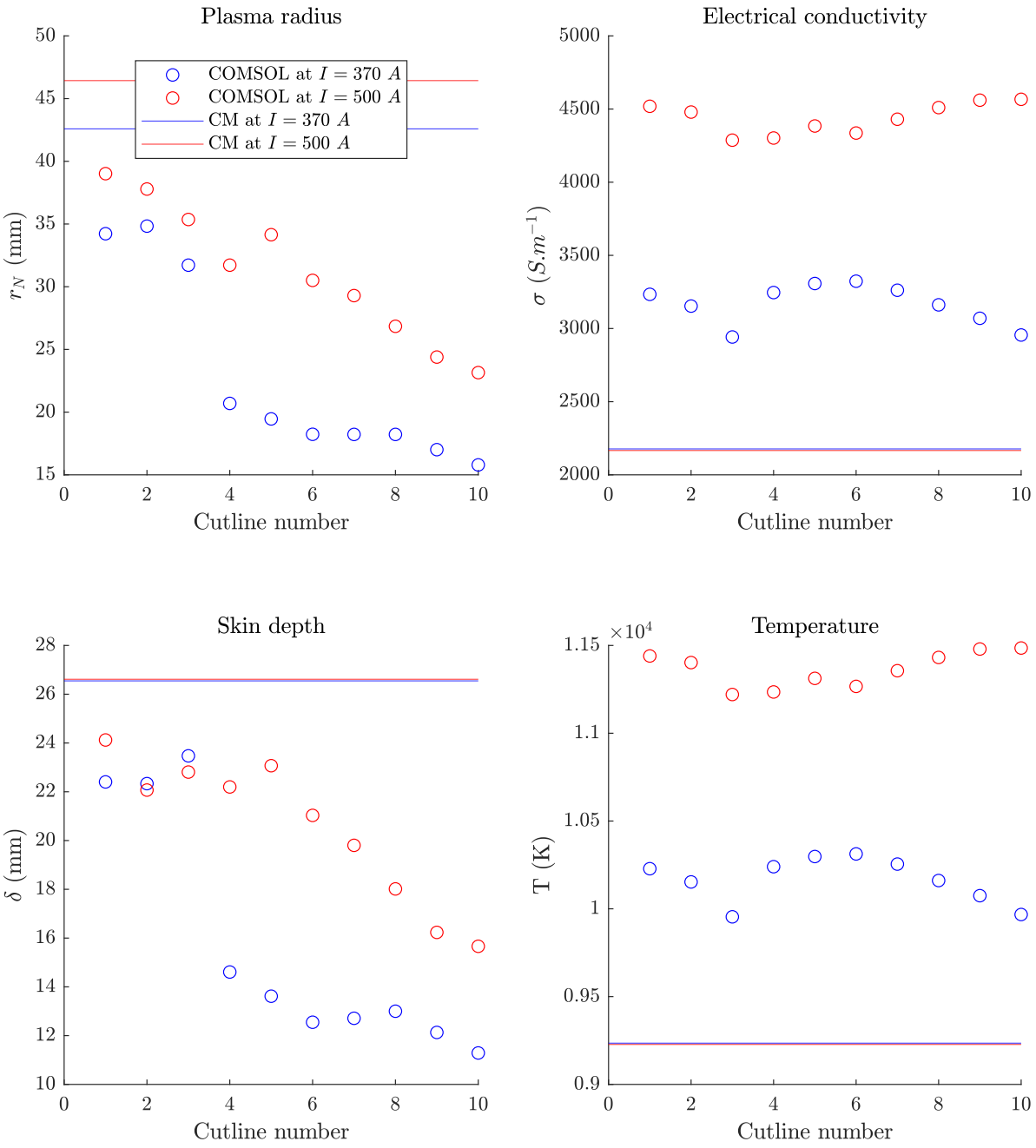

Figure 13. Plasma parameters calculated and averaged along the cutlines.

4.3. Comparison between COMSOL results and CM: 2.1 MHz *nitrogen case*

Similarly to the previous section, we make use of COMSOL simulations to compare output results with the ones from the channel model. The simulations are run at different burner diameters D, once at constant volume flow rate Q and once at constant velocity Vz. The coil length is constant: $L_c = 100\ mm$, and the coil gap to the burner wall is also constant ($7\ mm$), so that $R_c = D/2 + 7\ (mm)$. Radial temperature profiles (not shown in the table) from COMSOL are extracted along a cutline defined in front of the

coil center, from $r = 0\ mm$ to $r = R$. The plasma radius r_N is defined as the location, along this cutline, where the maximum power from the coil is deposited into the plasma. Data from COMSOL is summarized in table 7. The column $1/\xi$ represents the "quality factor", where ξ from COMSOL is calculated as:

$$\xi = \frac{W_{\text{active}}}{W_{\text{reactive}}} = \frac{\Re(V \times I^*)}{\Im(V \times I^*)} = \frac{\text{Coil resistance}}{\text{Coil reactance}} \tag{12}$$

Table 7. Results from COMSOL simulations for N_2 at 2.1 MHz. Coupled power: $W = 100\ kW$. Coil length: $L_c = 100\ mm$. Coil radius: $R_c = D/2 + 7\ (mm)$.

	Q const				**Vz const**			
$D\ (mm)$	$I_{\text{RMS}}\ (A)$	$B\ (mT)$	$r_N\ (mm)$	$1/\xi$	$I_{\text{RMS}}\ (A)$	$B\ (mT)$	$r_N\ (mm)$	$1/\xi$
50	518	27.2	12	25	461	24.2	14	19.5
70	424	21.1	16	26	408	20.3	16	24.5
90	360	17.1	17	27	360	17.1	17	27
110	298	13.5	19	25	310	14.0	19	27
130	246	10.6	27	22	270	11.6	24	26

Let us first compare the usual magnetic intensity H_0, shown in figure 14. The discrepancy between COMSOL and CM is of a factor 5 to 6, similar to the previous cases reported. Figure 15 shows the CM calculations for the plasma radius r_N vs the location of the maximum deposited power in COMSOL. Like for the results presented in the previous section, the plasma radius calculated by the channel model is very close to the burner radius values, a characteristic of the asymptotic behavior described before. This is not realistic and does not allow one to assess the validity of the channel model. Consequently, we attempt to derive an "equivalent plasma radius", where the COMSOL radial temperature profiles along the cutline facing the coil center are used. This new plasma radius definition r_{eq} is built in a way that the averaged temperature from $r = 0\ mm$ to $r = r_{\text{eq}}$ is equal to the temperature calculated with the channel model:

$$r_{\text{eq}} \text{ such that } \frac{1}{r_{\text{eq}}} \int_0^{r_{\text{eq}}} T_{\text{COMSOL}}(r) dr = T_{\text{CM}} \tag{13}$$

Results of this new definition for the plasma radius are displayed in figure 16. The agreement between absolute values becomes very good, which may indicate that the equations from the channel model are valid in terms of power balance and averaged temperatures. However, this seemingly great match must be considered with caution:

(i) The absolute values are very close to the maximum value possible, $\max(r_N) = R$. Consequently, the channel model does not provide any useful insight regarding the plasma radius ; it is simply very close to the burner radius.

(ii) If we could estimate the shape of the radial temperature profile only from the averaged temperature, the excitation frequency and the burner radius, then we could use the CM to assess temperature distribution in any Ar/N_2 ICPs with

different geometries and operating conditions. This ideal case is unfortunately not possible at the moment: it is too complicated to have one fitting function predicting the radial temperature profiles only from R, ν and gas type. Therefore, COMSOL can be used to predict the CM results, but not the opposite, which is not useful in our context.

Similarly, we derived equivalent plasma radiuses to obtain the same coupling with CM as the coupling given by COMSOL (not shown in this report). However, we face the same issue as before: it requires detailed simulations from COMSOL to obtain corrected values in the channel model, hence not applicable.

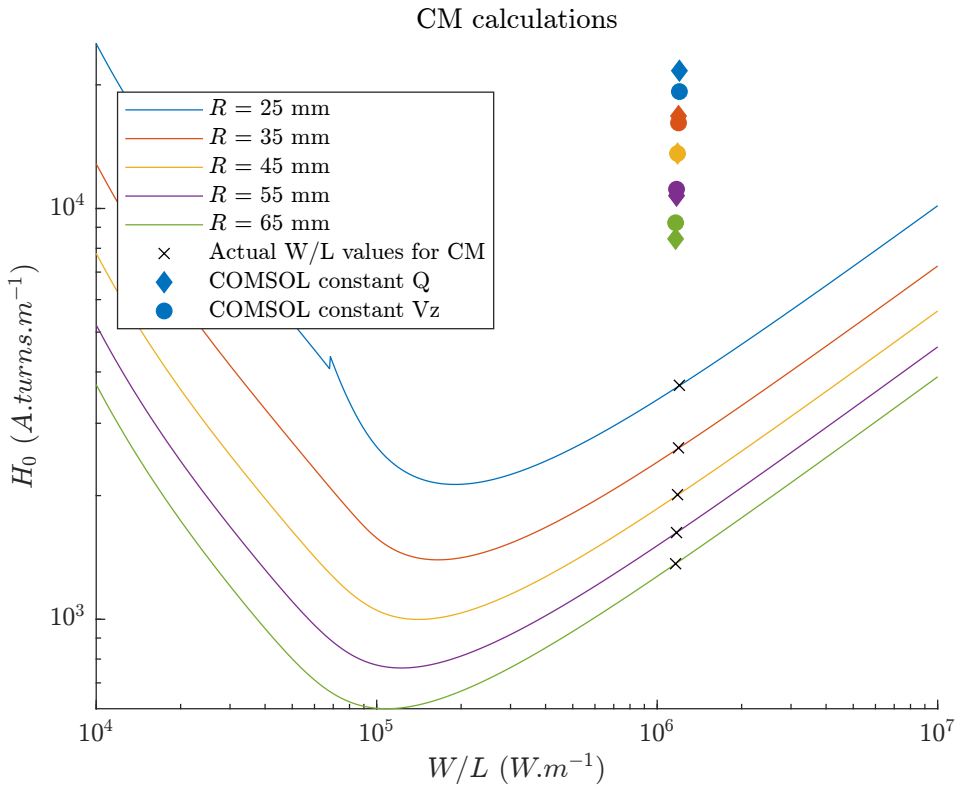

Figure 14. Caption

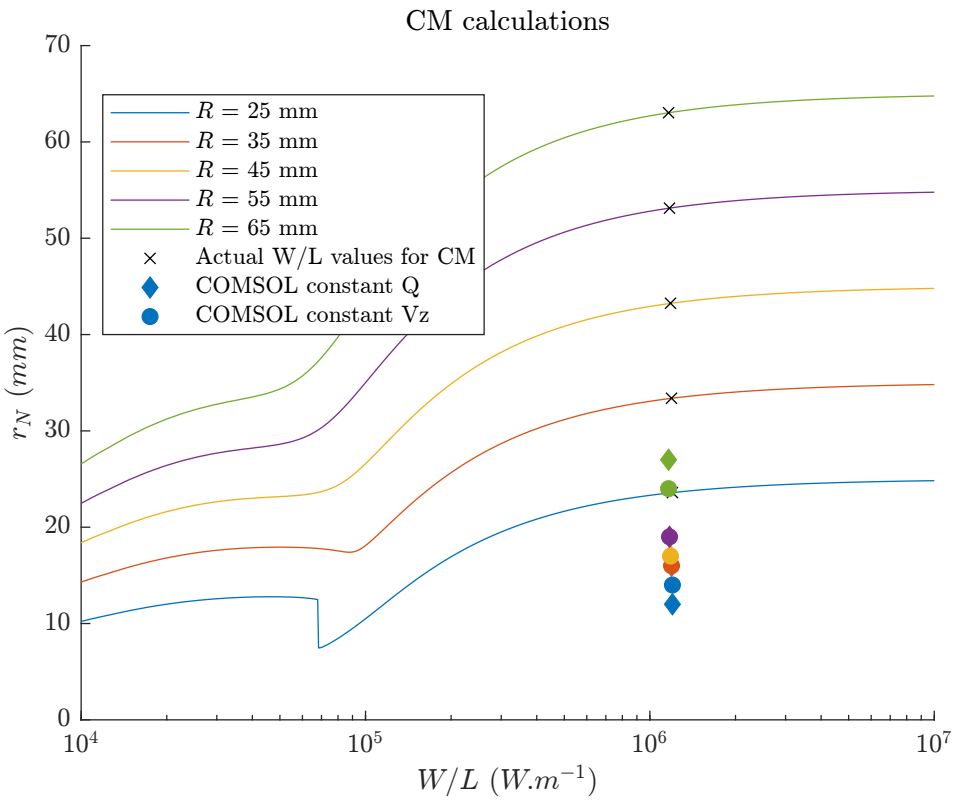

Figure 15. Caption

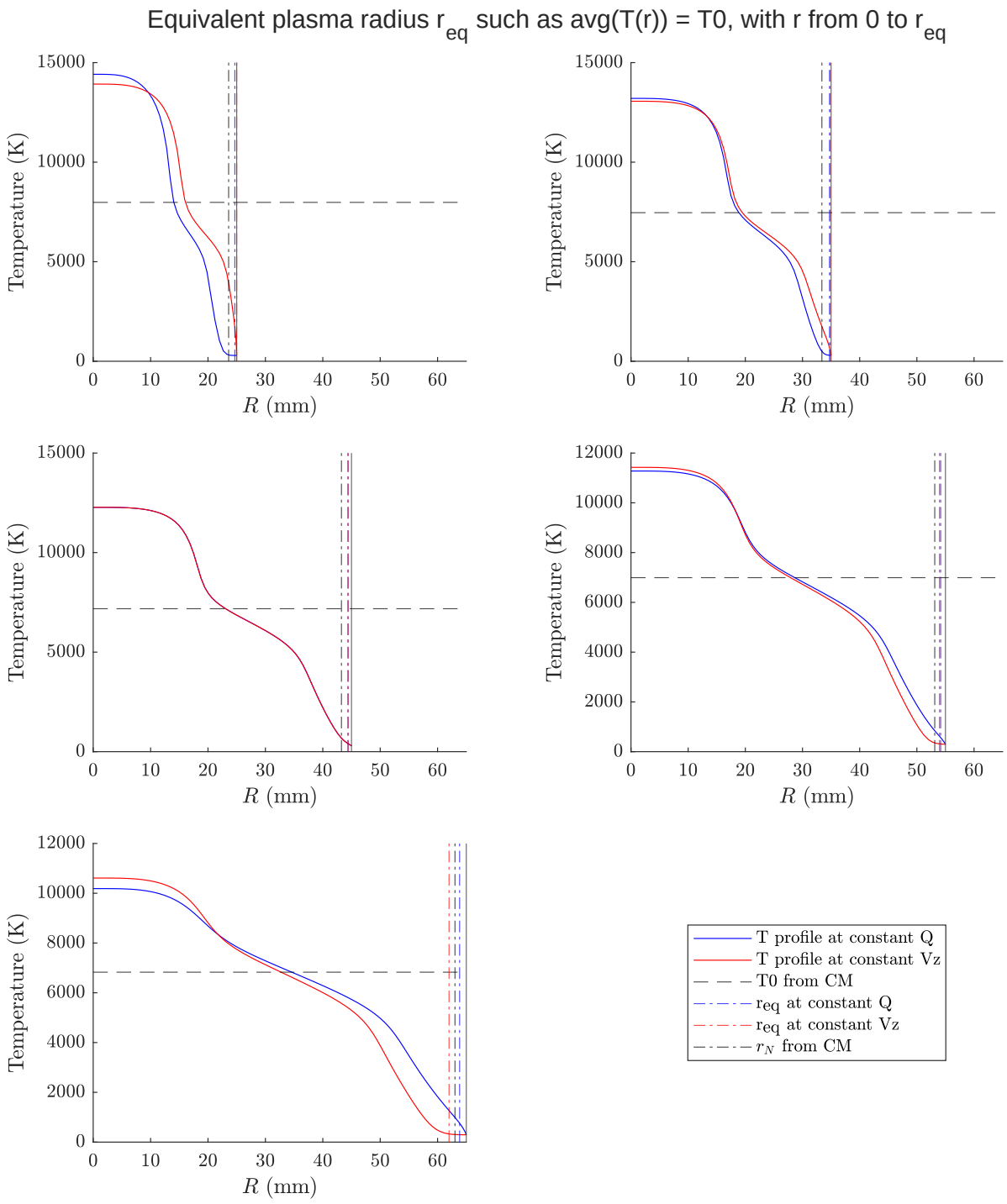

Figure 16. Plasma radius from CM and equivalent radius from COMSOL, for different burner radiuses R. The temperature profiles are calculated in COMSOL along a radial cutline facing the center of the coil.

4.4. Application to N_2 *for varying radiuses and frequencies*

[Corresponding report: 20th of June 2024.]

We present here one possible application of the channel model, where we want to characterize the main plasma parameters when the burner radius and the frequency are modified. We focus specifically on the coupling coefficient, defined in section 4. This virtual case represents a high-power long torch for heating applications. Table 8 summarizes the CM inputs with the default values for R_{burner} when ν changes, and reciprocally. All results were calculated using COMSOL thermal and electrical conductivities for the gas. Interestingly, κ naturally tends to its optimum value at high linear powers: $\kappa = \sqrt{2}\rho \rightarrow \sqrt{2}\rho_{\text{lim}} \simeq 2.5$. Note that, with the model from Freeman and Chase, it is impossible for κ to takes values above the threshold of 2.515, so that for tight coupling between the burner and the coil the optimum value will never be reached.

Table 8. Default values for the varying burner radius and frequency studies.

Gas	L_c (mm)	R_c (mm)	R (mm)	ν (Hz)	P (kW)
N_2	200	$R+7$	60	200×10^3	750

4.4.1. Burner radius variations

Here we report the variations of key parameters when the burner radius is varying from 50 mm to 100 mm with 10 mm steps. The black circles in figure 17 and figure 18 indicate the corresponding linear power W/L for each condition. Although the plasma power is identical in all calculations, the equivalent plasma length L is slightly changing because the ratio $R/R_{\text{coil}} = R/(R+7[mm])$ used to calculate κ_T is changing with the burner radius. In practice, $\min(\kappa_T) = 0.908$ and $\max(\kappa_T) = 0.919$, so the difference is very small.

From figure 17, we see that the coupling coefficient is increasing with the burner radius. This is an expected result: with conditions described in 8, we always have $\kappa \simeq 2.5$. Consequently, the major influence on the coupling coefficient is from the ratio $r_N/R_c \simeq R/(R+7)$. The higher the burner radius, the closer r_N/R_c is to 1, hence the higher the coupling coefficient. The curve at $r_N/R_c = 1$ gives the maximum obtainable value, which is $\simeq 0.6$.

From figure 18, we observe an asymptotic behavior of δ depending only on the burner radius, such that $\delta_{\text{lim}} = R/\rho_{\text{lim}}$. This is a non-intuitive result, as one would expect the frequency to be the main influence on the skin depth. The relevance of this behavior is debatable and may exists only because of the crudeness of the channel model. Similarly, σ has an asymptotic behavior depending on both the burner radius ($\sigma_{\text{lim}} \sim R^{-2}$) and the frequency ($\sigma_{\text{lim}} \sim \nu^{-1}$). For these high linear power values, the absolute value of r_N/R does not vary much and is very close to 1. Two important non-intuitive results are shown here: increasing the burner radius (at constant coil gap) reduces the magnetic field intensity required for operation, and in parallel lowers the

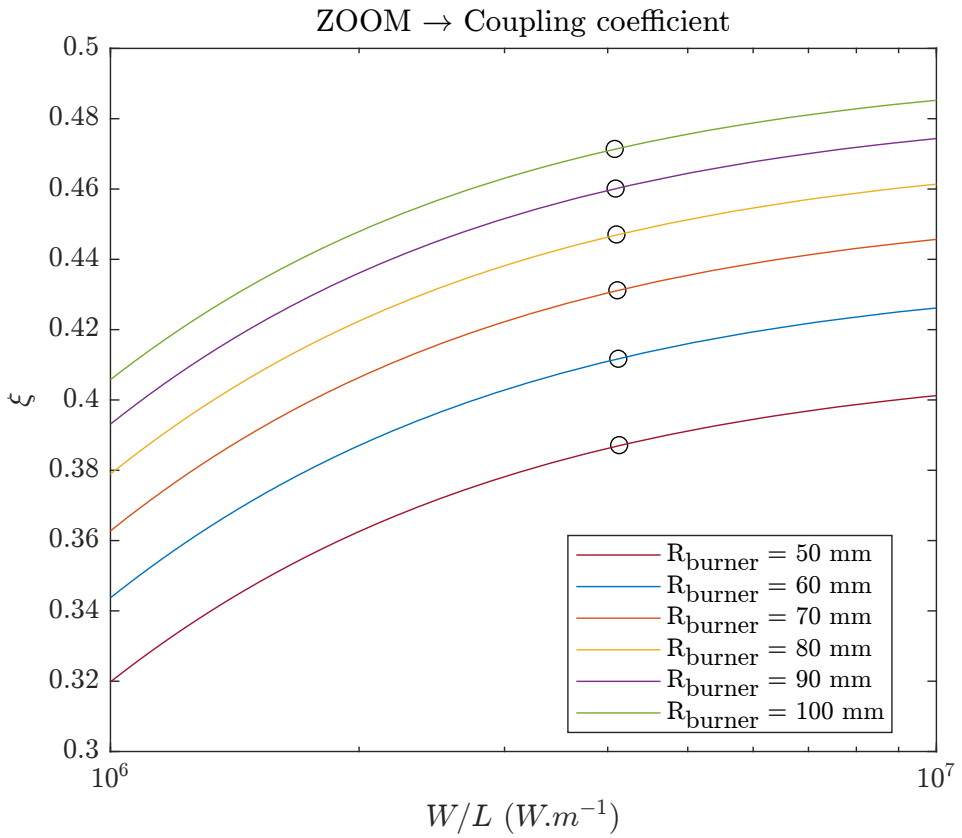

Figure 17. Coupling coefficient for the burner radius variations.

average temperature of the plasma. Whether this is consistent or not would require additional experiments or simulations.

4.4.2. Frequency variations

Here we report the variations of key parameters when the frequency is varying from 70 kHz to 310 kHz with 40 kHz steps. The coupling coefficient, shown in figure19, is slightly increasing with the frequency, but its variation is much less important than for the burner radius study. In the limit $r_N/ \rightarrow R$, we have $r_N/R_c \simeq 0.90$, so the maximum of the coupling coefficient is obtained at $\kappa \simeq 4$. However, the channel model limits possible values of κ to 2.515. Hence very small variations of the coupling coefficient, considering that δ and r_N values do not change much, as seen in figure 20.

From figure 20, we confirm the well-known fact that increasing the frequency reduces the magnetic field intensity required for plasma operation. Therefore, the plasma temperature is also reduced at higher frequencies.

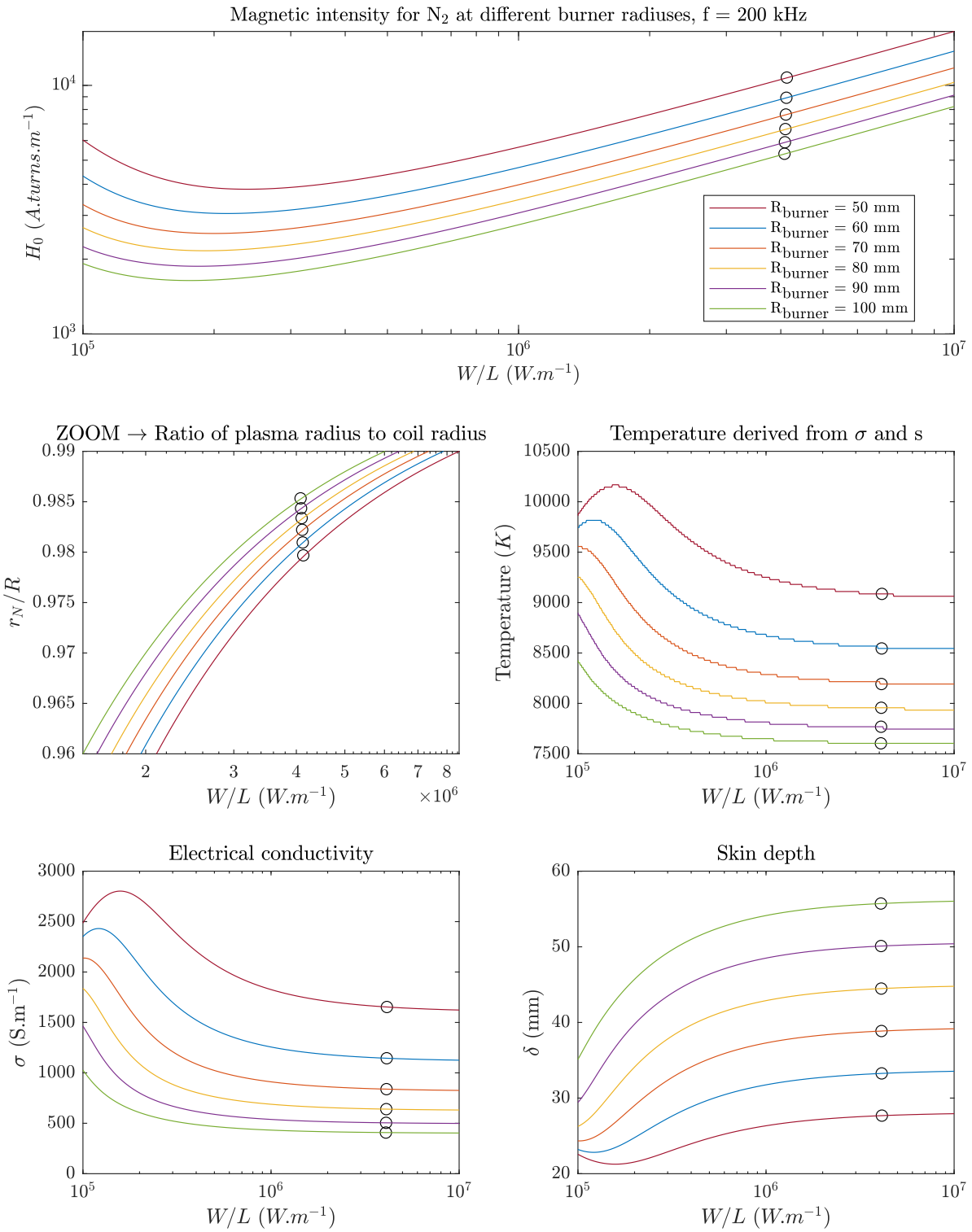

Figure 18. Main plasma parameters for the burner radius variations.

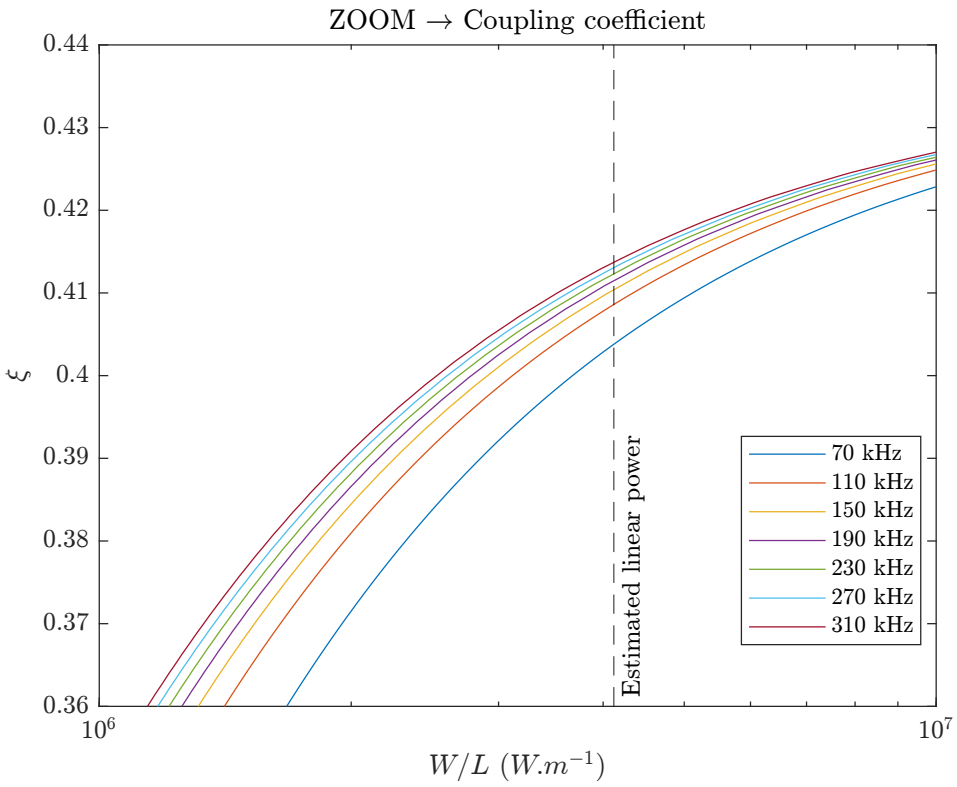

Figure 19. Coupling coefficient for the frequency variations.

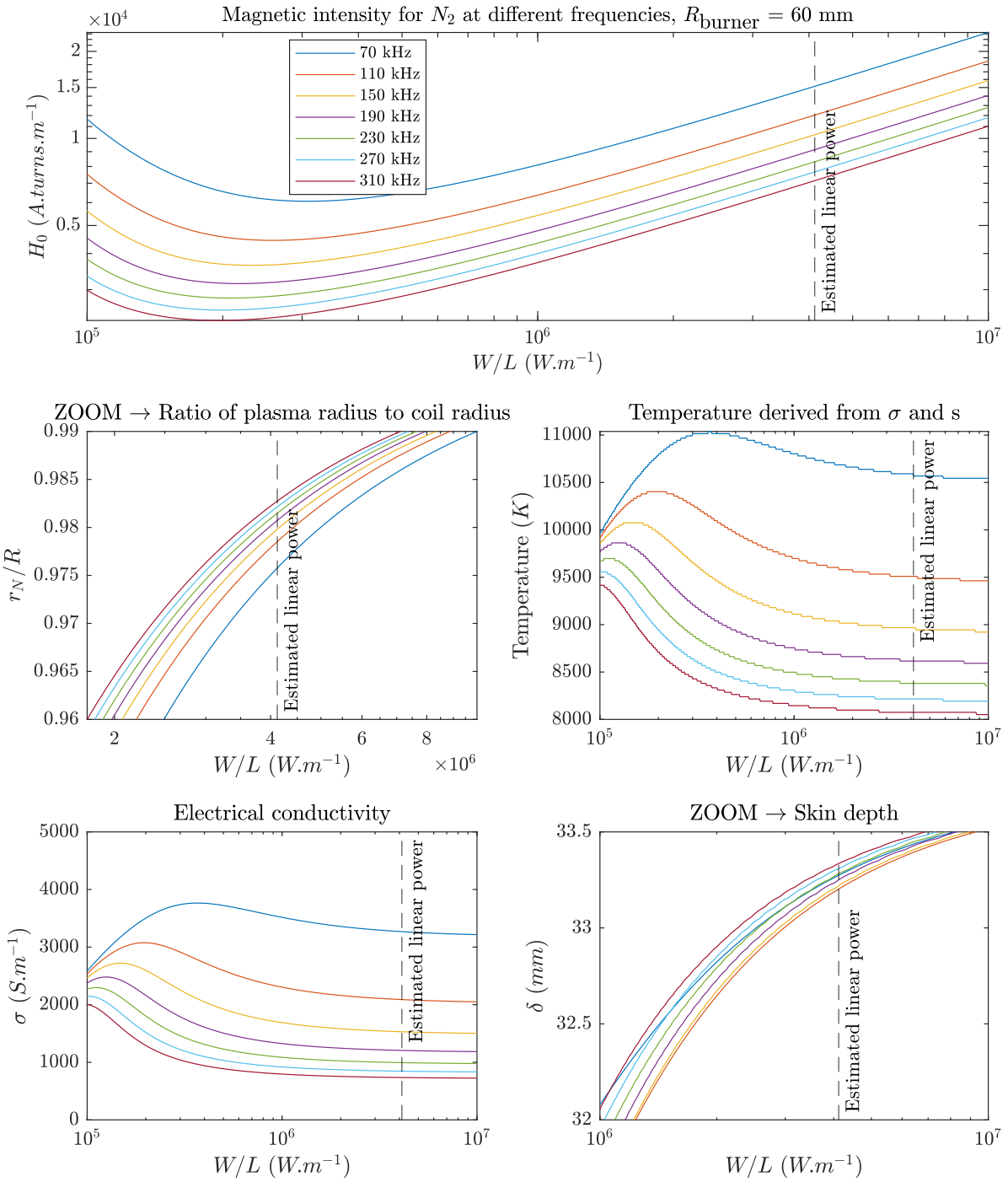

Figure 20. Main plasma parameters for the frequency variations.

5. Conclusion

The model derived by Freeman and Chase was successfully implemented on MATLAB and its use was extended to new gases and coupling coefficient. However, the agreement with experiments or COMSOL simulations is, in general, rather poor. Consequently, and as claimed by the authors themselves, it can barely be used for any quantitative study at the moment. The necessary efforts to improve the model seem not justified in our opinion: (i) the original goal of simplicity would be lost, (ii) it is difficult to identify what modifications would fit.

Nevertheless, it is still a useful tool for qualitative studies and relative comparisons. For instance, it can be used to investigate the change in plasma properties when using different gases. Alternatively, assuming that one manages to properly characterize the discrepancy between the CM and experiments (within a restricted range of operation), the model could also provide insightful data by extrapolation. Proceeding this way should be done carefully though.

Hereafter we briefly mention some unsuccessful studies with the CM and we summarize the current state of the solver and its outputs.

Unsuccessful studies

Thanks to the data provided by S. Eizaguirre, we investigated different ways to reduce the discrepancy between COMSOL simulations and CM predictions. Because the channel model outputs correspond, by definition, to averaged quantities, a lot of efforts were dedicated to find "equivalent" averaged quantities in COMSOL. For the sake of clarity, we do not include the corresponding figures and discussions in this report. We considered different plasma radius definitions, focused on the conductive heat at the walls rather than the total coupled power, defined domains restricted to the coil region, etc. In summary, two main problems arise:

(i) Any correction factor, or "equivalent" quantities, giving interesting agreement between COMSOL and the CM is too context-dependent. If the gas, frequency, burner radius, flow type, etc. is changed, then the agreement is lost. Some "similarity laws" could help but are beyond the scope of this report in our time frame.

(ii) Often, the detailed data from COMSOL can be related to the averaged quantities of the CM (*e.g.* in 4.3) by applying some data transformation. However, our goal is the opposite here: we want to make use of the predictive capability of the channel model to avoid relying heavily on detailed numerical simulations.

Available gases

The current code can handle the following gases:

- Argon - 'Ar' with two sets of inputs available: 'Freeman' and 'COMSOL' (recommended).

- Nitrogen - 'N2' with two sets of inputs available: 'Freeman' and 'COMSOL' (recommended).
- Oxygen - 'O2' with one set of inputs available: 'COMSOL'.
- Iron - 'Fe' with one set of inputs available: 'Cressault'.
- Iodine - 'I2' with one set of inputs available: 'Murphy'.

Note that as long as we do not have a "mixing rule" (or Chapman-Enskog procedure) for the conductivities, we can not apply the model to mixtures.

Data tables

The solver was run for different input parameters in order to create detailed data tables. The goal is to obtain immediate results by interpolation rather than running the solver every time. Currently, the interpolated tables used the following inputs:

- Gases: argon and nitrogen.
- Origin of the conductivities: COMSOL.
- Linear power range: $[10^4\ W.m^{-1}\ ;\ 10^7\ W.m^{-1}]$ logarithmically spaced with 1000 points.
- Burner radius range: $[15\ mm\ ;\ 120\ mm]$ by steps of 1 mm.
- Frequency vector: $[10\ kHz\ ;\ 13.56\ MHz]$ logarithmically spaced with 50 points.

Extra functionality

We created a function **determineOptimumCoupling.m** giving the optimum coupling value vs burner radius. A deviation threshold ε can be entered to observe how the main plasma quantities vary if the burner radius is modified by $R(1 \pm \varepsilon)$. The required inputs are the classic ones for the channel model, plus the coil gap to calculate the coupling coefficient.

Flow chart

Figure 21 shows the basic principle of CM utilization, including the coupling coefficient from [3].

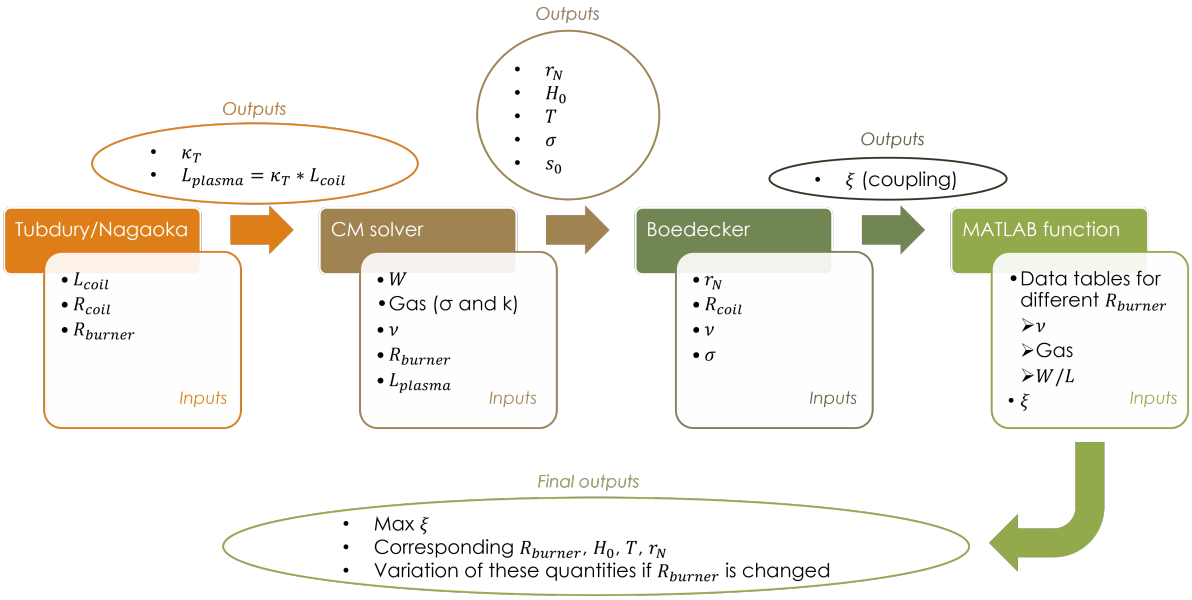

Figure 21. Flow chart of CM utilization.

References

[1] M. P. Freeman and J. D. Chase. Energy-transfer mechanism and typical operating characteristics for the thermal rf plasma generator. *Journal of Applied Physics*, 39(1):180–193, 1968.

[2] P.G. Simpson. *Induction Heating: Coil and System Design*. McGraw-Hill, 1960.

[3] A. E. Mensing and L. R. Boedecker. *Theoretical investigations of R-F induction heated plasmas*. National Aeronautics and Space Administration, 1969.

[4] M. L. Thorpe and L. W. Scammon. Induction plasma heating - high power, low frequency operation and pure hydrogen heating. Technical report, Humphreys Corporation, 1969.

[5] M. I. Boulos, P. L. Fauchais, and E. Pfender. *Handbook of Thermal Plasmas*. Springer Cham, 2023.

[6] C.A. Tudbury. *Basics of Induction Heating*. Number vol. 1 in A Rider publication. J. F. Rider, 1960.

[7] M. Kennedy, S. Akhtar, J. Bakken, and R. Aune. Review of classical design methods as applied to aluminum billet heating with induction coils. *TMS Annual Meeting*, 2011.

[8] J. W. Poole, M. P. Freeman, K. W. Doak, and M. L. Thorpe. Simulator test to study hot-flow problems related to a gas core reactor. *NASA CR-2309*, 1973.